Journal of Biomedical Optics

SPIEDigitalLibrary.org/jbo

Two-dimensional and three-dimensional viability measurements of adult stem cells with optical coherence phase microscopy

Pierre O. Bagnaninchi
Christina Holmes
Nicola Drummond
Jamal Daoud
Maryam Tabrizian

Two-dimensional and three-dimensional viability measurements of adult stem cells with optical coherence phase microscopy

Pierre O. Bagnaninchi,[a] Christina Holmes,[b] Nicola Drummond,[a] Jamal Daoud,[b] and Maryam Tabrizian[b]
[a]University of Edinburgh, MRC Centre for Regenerative Medicine, Edinburgh, United Kingdom
[b]McGill University, Department of Biomedical Engineering, Montreal, Canada

Abstract. Cell viability assays are essential tools for cell biology. They assess healthy cells in a sample and enable the quantification of cellular responses to reagents of interest. Noninvasive and label-free assays are desirable in two-dimensional (2D) and three-dimensional (3D) cell culture to facilitate time-course viability studies. Cellular micromotion, emanating from cell to substrate distance variations, has been demonstrated as a marker of cell viability with electric cell-substrate impedance sensing (ECIS). In this study we investigated if optical coherence phase microscopy (OCPM) was able to report phase fluctuations of adult stem cells in 2D and 3D that could be associated with cellular micromotion. An OCPM has been developed around a Thorlabs engine ($\lambda o = 930$ nm) and integrated in an inverted microscope with a custom scanning head. Human adipose derived stem cells (ADSCs, Invitrogen) were cultured in Mesenpro RS medium and seeded either on ECIS arrays, 2D cell culture dishes, or in 3D highly porous microplotted polymeric scaffolds. ADSC micromotion was confirmed by ECIS analysis. Live and fixed ADSCs were then investigated in 2D and 3D with OCPM. Significant differences were found in phase fluctuations between the different conditions. This study indicated that OCPM could potentially assess cell vitality in 2D and in 3D microstructures. [DOI: 10.1117/1.3606561]

Keywords: optical coherence phase microscopy; cell motility; three-dimensional scaffold; tissue engineering; phase fluctuations.

Paper 11009PRR received Jan. 7, 2011; revised manuscript received Jun. 8, 2011; accepted for publication Jun. 8, 2011; published online Aug. 1, 2011.

1 Introduction

Numerous strategies have been designed over the years to analyze cellular viability. Cell viability assays are essential to enable the quantification of cellular responses to reagents of interest. The two most prominent of which are based either on the cell membrane integrity (dye exclusion assays), or on the formation of a side product characteristic of cellular metabolic activity. In general, these assays are destructive and prevent time-course studies of cell vitality.

Healthy cells are also characterized by a constant motility resulting from a continuous rearrangement of focal adhesion points and cell shape fluctuations. Even when confluent healthy cells exhibit a vertical micromotion that was demonstrated by measuring their electrical activity on gold microelectrodes.[1,2] Microtion is defined by nanoscale displacements as opposed to larger cell motility events. Since then, the electric cell-substrate impedance sensing (ECIS) technique has been established as a novel noninvasive mean to assess cell vitality.

Increasingly, cells are cultured in 3D environments, which have been demonstrated to enable cellular physiological functions to more closely resemble those of *in vivo* models.[3] In addition, regenerative medicine and tissue engineering techniques aim toward developing replacement tissues from cells cultured in 3D structures. In 3D, noninvasive cell vitality assays are generally restricted to the use of fluorophores in combination with confocal or two-photon fluorescence microscopy. However, cell autofluorescence measured by two-photon fluorescence can correlate to cell viability.[4,5]

Quantitative phase imaging modalities, such as digital holographic microscopy[6,7] or Fourier phase microscopy,[8,9] have a nanoscale sensitivity that has been exploited for live cell *en face* topographic imaging and analysis. In 3D, coherence-domain digital holography has been exploited to measure cellular motility in tumor spheroids.[10]

Optical coherence tomography (OCT) is also an interferometric imaging modality that has the advantage of producing cross-sectional imaging. OCT can achieve micrometer resolution within a 3D millimeter volume without the use of any external labeling to enhance contrast.[11–13] It works in a similar way to ultrasound imaging by measuring backscattered light delays instead of acoustic wave delays. While the lead clinical application is in ophthalmology, where the penetration depth is less of an issue, OCT has also shown promise in developmental biology[14] and in the field of tissue engineering.[15–18] Finally, the latest common-path optical coherence microscope[19–23] can achieve quantitative phase contrast images with an unprecendented phase stability, thus allowing the capture of subwavelength information and the mapping of the optical thickness of a single cell at a nanometer level, while keeping its optical sectioning ability.

The aim of this study was to investigate whether optical coherence phase microscopy (OCPM) could assess adult stem

Address all correspondence to: Pierre O. Bagnaninchi, University of Edinburgh, MRC Centre for Regenerative Medicine, 49 Little France Crescent, EH16 4SB Edinburgh, United Kingdom; Tel: +44131 242 61 64; E-mail: pierre.bagnaninchi@ed.ac.uk.

1083-3668/2011/16(8)/086003/8/$25.00

cell viability in 2D and 3D by analyzing phase fluctuations that could be correlated to cell motility.

2 Materials and Methods

2.1 *Optical Coherence Phase Microscopy*

In the system used for this study, the light source and the spectrometer were parts of a commercial OCT engine (Callisto, Thorlabs). The superluminescent diode (SLD) is centered around 930 nm with a FWHM bandwidth of 90 nm. The resolution given by the manufacturer is 7 μm in air, corresponding to 5 μm in tissue. The spectrometer recorded 1200 spectra per second.

The light was coupled out of the OCT engine into a single mode fiber and collimated onto a pair of galvanometers for raster scanning. The custom scanning head was attached to an inverted microscope (SPi95, Brunel microscope) and delivered to a 10× objective (NA = 0.17) or a 20× (NA = 0.4).

As such, the system was in a common path set-up [Fig. 1(a)] without reference arm as in a conventional Michaelson interferometer. Instead, a strong reflection within the sample arm was used as the reference. As a result, there was an increase in phase stability as common noise (i.e., differences of temperature between reference and sample arms, vibrations, fluctuations) was more efficiently rejected.

The backscattered light reflected from within the sample interfered with the reference reflection, generally the bottom surface of a coverslip, perpendicular to the laser beam, onto which the cells were directly cultured. These interferences were traveling along the same path back to the spectrometer. A spectrum was measured at each x,y point of the sample by raster scanning.

In spectral domain OCT, the interferences between the sample and the reference arms were spectrally dispersed and measured at each k with the spectrometer. As a result, we observed a modulation of the light source spectrum. The spectral intensity $I(k)$, a function of the wavenumber k, is given by

$$I(k) = \Gamma_r S(k) + \Gamma_s S(k) + 2S(k)\sqrt{\Gamma_r \Gamma_s}\cos(2k\delta + \varphi), \tag{1}$$

where Γ_r is the reflectivity of the reference surface, Γ_s is the reflectivity of the sample, S(k) is the spectral density of the light source, δ is the optical path difference, and φ is an arbitrary phase.

The depth information profile, the A scan, originating from the light being scattered at a different depth within the sample, can be retrieved with an inverse Fourier transform. The discrete Fourier transform gives access to the intensity, $I(z)$, and the phase, $\Phi(z)$, of the light beam at different depths, z

$$\Phi(z) = tan^{-1}\left(\frac{\mathrm{Im}\{F[I(k)]\}}{\mathrm{Re}\{F[I(k)]\}}\right). \tag{2}$$

The intensity, $I(z)$, provides structural information from the sample. The phase, $\Phi(z)$ is related to the optical properties at the depth z

$$\Phi(z) = \frac{4\pi}{\lambda o} n[z + \delta z(t, x, y)], \tag{3}$$

where λo is the central wavelength of the source, n is the effective refractive index at the depth z, and $\delta z(t, x, y)$ represents spatial and temporal fluctuations in the path differences. In consequence of Eqs. (2) and (3), the phase is 2π wrapped every $\lambda o\,/(2n)$.

Phase stability determines the minimum phase variations above the noise floor that are detectable by the system. Theoretically, the phase variance can be calculated as[19,21]

$$\langle \Phi(z)^2 \rangle = \frac{1}{SNR}, \tag{4}$$

where SNR is the signal to noise ratio.

The phase stability was defined as the standard deviation, i.e., the square root of $\langle \Phi(z)^2 \rangle$. With a theoretical SNR of 83 db in air, the system had a theoretical phase stability of 7×10^{-5} radians. Note that SNR(db) = 10 log 10(SNR).

In the case of 2D imaging, only the top surface was of interest; whereas in 3D structures, the intensity and phase were measured within the depth of field of the objective used.

2.2 *Phase Fluctuations Measurements*

We measured phase fluctuations by collecting 50 successive B scans at the same location, yo. We collected 400 A scans in the x direction for 2D imaging and 500 for 3D imaging. At a scanning rate of 1200 s^{-1}, the phase $\Phi(\mathrm{ti}, x, yo, z) = \Phi i(x, z)$ was measured every 0.33 s for 2D and 0.41 s for 3D imaging. Respectively, the total acquisition times were of 16.5 s and 20.5 s.

The phase fluctuations were defined as

$$\delta\Phi(x, z) = \Phi i + 1 - \Phi i = \frac{4\pi}{\lambda o} n\delta z, \tag{5}$$

where i = [1,...,49] is indexing the number of B scans. The maximum of the phase fluctuations, or the standard deviation of $\delta\Phi$ over the acquisition time interval, were analyzed.

2.3 *Cell Culture*

Human adipose derived stem cells (ADSCs) (Invitrogen) were expanded to passage two in a low serum medium (complete RS MesenPRO) with 2 mM L-glutamine according to the supplier protocol and cultured onto glass coverslips at least one day prior to imaging in a humidified incubator at 37° and 5% CO_2.

2.4 *Three-Dimensional Cell Culture*

2.4.1 *Scaffold fabrication*

Three-dimensional (3D) scaffolds were fabricated from poly(DL-lactide-co-glycolide) acid (PLGA; 85 Mole% DL-lactide, 15 Mole% glycolide; MW = 92 to142 kDa; Lakeshore Biomaterials, Birmingham, USA) using an XYZ bioplotter system (Envisiontec, Gladbeck, Germany) previously described by Landers et al.[24] The PLGA was dissolved in methyl ethyl ketone (Sigma) at a 1:1 ratio of PLGA to solvent and subsequently mixed with 15% w/w sodium chloride (NaCl), sieved to yield a particle size distribution of 53 to 63 nm. The PLGA solution was transferred to the plotting cartridge and was dispensed layer by layer, forming a 0 deg/90 deg strand structure 40×40 mm-wide and 3.6 mm-thick, using a CAD file as a template. To yield a strand diameter (D) of 150 μm, 250 μm-diameter dispensing tips were used at a dispensing speed of 165 mm/s.[25] The layers were overlaid to give a strand thickness (h) of 120 μm and a layer spacing distance, L, of ~300 μm. Individual scaffolds were punched from the initial scaffold brick using a

biopsy punch, yielding disks 8 mm in diameter and 3.6 mm-thick. These scaffolds were then immersed in water at 50 °C for up to 6 h in order to leach out the salt particles, air-dried for 24 h, and vacuum-dried for 48 h to allow for the complete evaporation of the solvent/water.

2.4.2 *Scaffold cell seeding*

Prior to cell seeding, scaffolds were immersed in a 70% ethanol solution for 1 h, rinsed twice in phosphate buffered saline (PBS) and then UV sterilized for 30 min. ADSCs were dynamically seeded into the scaffolds, via an orbital shaker at 37 °C and 50 rpm. Each scaffold was placed in a centrifuge tube containing 3 mL of ADSC-containing culture media at a concentration of 10^6 cells/mL. After 4 h of dynamic seeding, scaffolds were placed in 12 well tissue culture plates, culture medium was changed, and the 3D cell constructs were kept in a humidified incubator at 37° and 5% CO_2 until imaging.

2.5 *Electric Cell-Substrate Impedance Sensing*

A commercial ECIS system (ECIS Zθ, Applied Biophysics) was used to demonstrate that ADSCs experienced a continuous micromotion. The time and frequency dependent complex impedance, $Z(t, f)$, of the electrode-cell interface was recorded at multiple frequencies. Cells were grown on eight-well ECIS arrays containing one 250-μm gold microelectrode per well. Measurements were performed directly in the cell culture medium allowing real-time monitoring, while both the ECIS arrays and the measurement station were kept in an incubator with high-humidity at 37 °C and 5% CO2.

The real part of the impedance, $R(t, f)$, was normalized and filtered to remove DC components. The fast Fourier transform $[R(t, f)]$, was used to calculate the instantaneous power spectral density (PSD) and plotted on a log-log scale. A micromotion slope was determined by linearly fitting the low frequency part of the PSD.

3 Results

3.1 *Measured Phase Sensitivity*

Figure 1(b) shows a typical B scan, acquired with the OCPM, of a glass coverslip with cell culture medium on top. The top surface appeared as a bright line in the B scan. The corresponding A scan (in depth profile) at $x = 200$ is represented in

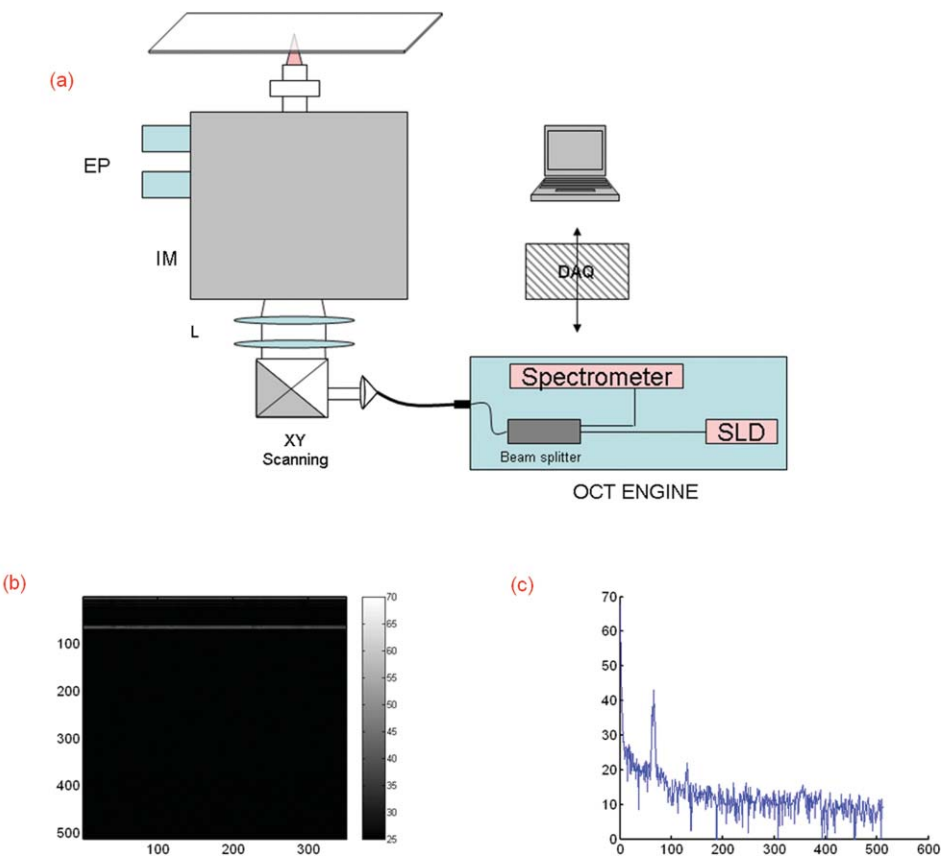

Fig. 1 (a) Schematic of the optical coherence phase microscope. A superluminescent light source (SLD) was sent to a custom scanning head attached to an inverted microscope. The interferences between a reference reflection and the light backscattered within the sample were measured as a modulation of the spectrum with a spectrometer. The light source and the spectrometer were part of a commercial OCT engine (Thorlabs). (b) Representative B and A scans (c) of a glass coverslip covered with cell culture medium measured by the OCPM. In (b), we can see the top surface of the cover slip appearing as a bright line. This line corresponds to the peak in the A scan (c). The intensity is reported in db.

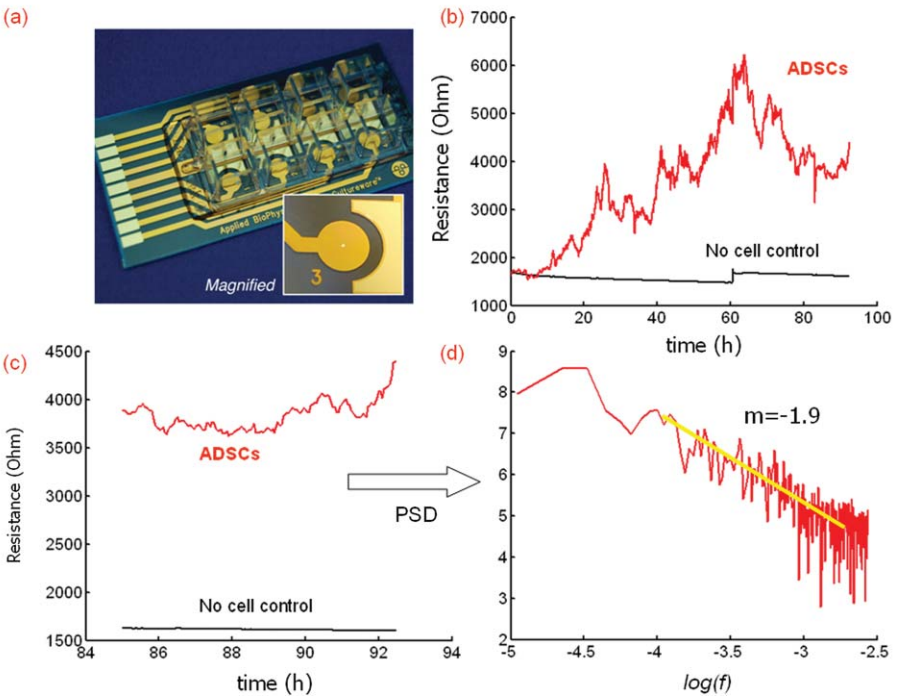

Fig. 2 (a) ADSCs were cultured on top of 250-μm gold microelectrodes (image reproduced from www.appliedbiophysics.com). (b) Recorded resistance of the cell-electrode interface. Fluctuations in the resistance were recorded even after cells reached confluency, demonstrating a constant activity termed as micromotion, and correlated to cell vitality. (c) Fluctuations in the resistance occurred at different time scales. (d) The slope of the PSD of these fluctuations was calculated at –1.9 and was similar to values reported for healthy cells. Cell-free controls had a PSD slope close to zero.

Fig. 1(c). In a liquid medium, the SNR is far below the theoretical one and was measured at ~35 db. Consequently, the measured phase sensitivity was on the order of 0.01 radians, which could be directly translated into a corresponding minimum measurable displacement of 0.56 nm by using Eq. (5). The OCPM was, therefore, able to measure any change in phase without ambiguity between 0.56 and 350 nm (for $n = 1.33$).

3.2 *Live Cells Display a Constant Micromotion*

The impedance of ADSCs cultured on gold microelectrodes [see Fig. 2(a)] displayed continuous multiscale fluctuations, as shown in Figs. 2(b) and 2(c). The impedance fluctuations were shown not to be due to electrical noise but to "biological noise." Typically for healthy cells, the slope of the power spectral density was measured between -1.9 and -2.1, which can be compared to a null slope for theoretical white noise or a no cell control. In this study, we measured a slope of -1.9 for ADSCs as shown in Fig. 2(d). The slope of the PSD fell to zero for ADSCs fixed in formalin. These results together with the measured phase sensitivity indicated that phase fluctuations corresponding to cellular micromotion could be measured for live ADSCs.

3.3 *Optical Coherence Phase Microscopy Two-Dimensional Imaging of Cells*

ADSCs were imaged on top of glass coverslips via OCPM by collecting 100 B scans in the y direction. In this particular case, only the top surface was of interest, as demonstrated in Fig. 1(b). At this depth, we reconstructed the intensity map, $I(x, y)$ [Fig. 3(a)], and the phase map, $\Phi(x, y)$ [Fig. 3(b)]. $I(x, y)$ was expressed in decibels and $\Phi(x, y)$ in radians. $\Phi(x, y)$ was within $[-\pi, \pi]$ and was not unwrapped on this image. The scanning step was set to 1.5 μm in the X direction (A scan) and to 3 μm in the Y direction (B scan). Both maps clearly showed general cell morphology. The resolution can be increased by switching to a 20× objective to reveal intracellular features as described in Ref. 23. However, in this study we were interested in optically averaging the phase fluctuations resulting from cellular micromotion, and we consequently settled for a lower optical resolution.

3.4 *Two Dimensional Phase Fluctuations*

We collected 50 B scans at the same y location and compared the phase fluctuations for live cells and cells fixed in formalin and stored overnight in PBS. The differences between live cells versus fixed cells were clear when plotting either the standard deviation [Fig. 4(a)] or the maximum of the discrete derivative of the phase at the same position x [Fig. 4(b)]. The maximum value has a direct physical meaning since it can be interpreted as a physical displacement, i.e., a vertical micromotion with Eq. (5).

The corresponding displacement scale was plotted on the right of the graph under the approximation that the refractive index is constant. It shows that the OCPM measured a maximum cellular displacement of 6 nm in this recording.

A few smaller phase fluctuations were recorded in cells fixed in formalin. They might be attributed to Brownian motion in

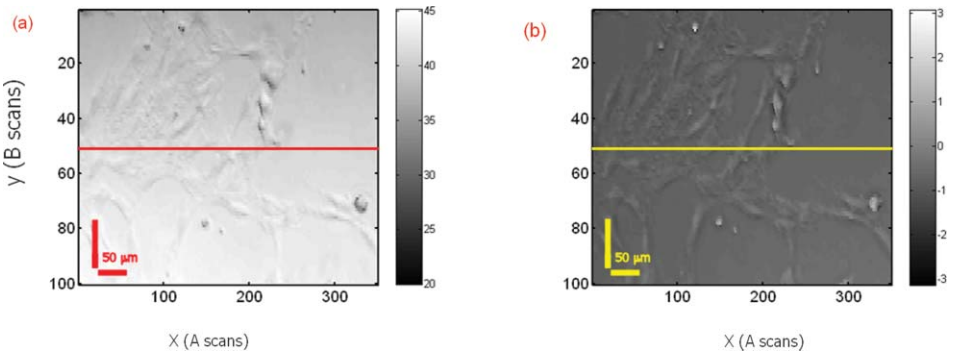

Fig. 3 (a) Intensity map, $I(x, y)$, of live ADSCs cultured on a glass coverslip. (b) Corresponding phase map, $\Phi(x, y)$. The phase was not unwrapped, and the displayed colorbar is in units of $[-\pi\ \pi]$. Scanning steps [Ascan (x), Bscan (y)] in these pictures were set to 1.5 μm × 3 μm. Corresponding 50-μm scale bars were plotted.

the fluid or other sources of phase noises. Note, however, the difference in spatial spreading between phase fluctuations that could be attributed to live cellular micromotion, and the spike appearance of $\delta\Phi$ for fixed cells.

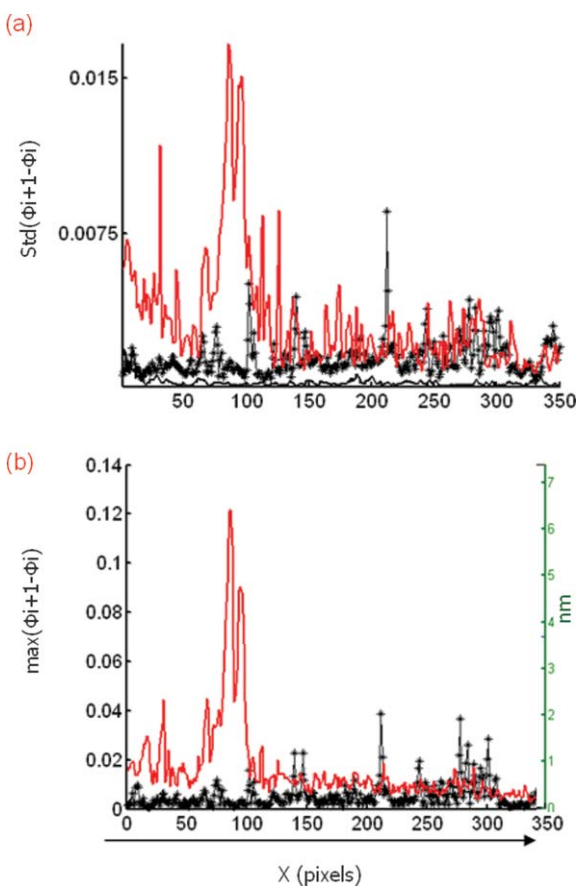

Fig. 4 (a) Plot of the phase fluctuations, $\delta\Phi$ standard deviation, along x calculated over a total acquisition time of 16.5 s at a 1200 s^{-1} acquisition rate. (b) Plot of the maximum of the phase fluctuations, $\delta\Phi$, with the same parameters. Live cells (plain line) were characterized by large cell fluctuations when compared to fixed cells (stars). The corresponding scale in nanometers is displayed on the right-hand side of the plot. Scanning steps [Ascan (x)] in these pictures were set to 1.5 μm.

3.5 *Three Dimensional Phase Fluctuations*

Figure 5(a) shows an OCPM B scan of a control scaffold without cells. The porous fibers running in the plane perpendicular to the page can be seen. 200 B scans were collected to reconstruct the sample in 3D. *En face* imaging [Fig. 5(b)] at a chosen depth, z, more clearly showed the structure of the fiber. In Fig. 5(c), the 3D structure of the cell-free sample was represented with open-source software (V3D).

For 3D phase fluctuation studies of cell-seeded scaffolds, we collected x-z cross-sections to image in depth within the sample. Statistics were performed over 50 cross-sections recorded at the same location $yo = 0$.

The mean intensities were represented in Figs. 6(a) and 6(b) for live and fixed 3D cell culture, respectively. The intensity pictures clearly revealed the fibers of the scaffold, displaying a similar structure to that observed in Fig. 5. In addition, we observed cells growing within the scaffold for both live [Fig. 6(a)] and fixed cells [Fig. 6(b)]. Based on the intensity pictures, no differences could be observed between the two conditions. In both cases, the cell-to-scaffold contrast resulted from an *a priori* knowledge of the cell-free structure.

However, when we plotted the standard deviation of the phase fluctuations, $\delta\Phi(x, z)$, of live [Fig. 6(c)] and fixed 3D cell cultures [Fig. 6(d)], we noted striking differences between live and fixed 3D cell culture. Only samples with live cells displayed a standard deviation of $\delta\Phi(x, z)$ above the background noise level. In these samples, the standard deviation of the $\delta\Phi(x, z)$ for the scaffold fibers were at the background noise level and, as a consequence, the cell-to-scaffold contrast was enhanced. No such contrast existed for fixed samples and both cells and scaffold displayed standard deviations under the noise threshold. Note that the phase and its derivatives were not calculated outside areas where the intensity was below the noise threshold. Hence, the image background of zero is artificial. In the phase fluctuations map, several spikes can be observed in live cells, scaffold material, and fixed samples. These spikes could be due to random phase instabilities and/or to phase wrapping creating a large shift in the phase derivative.

Similar to Fig. 4, the phase fluctuations of live cells were spatially spread over defined areas. This could be used advantageously to average over the noise represented by the phase fluctuation spikes.

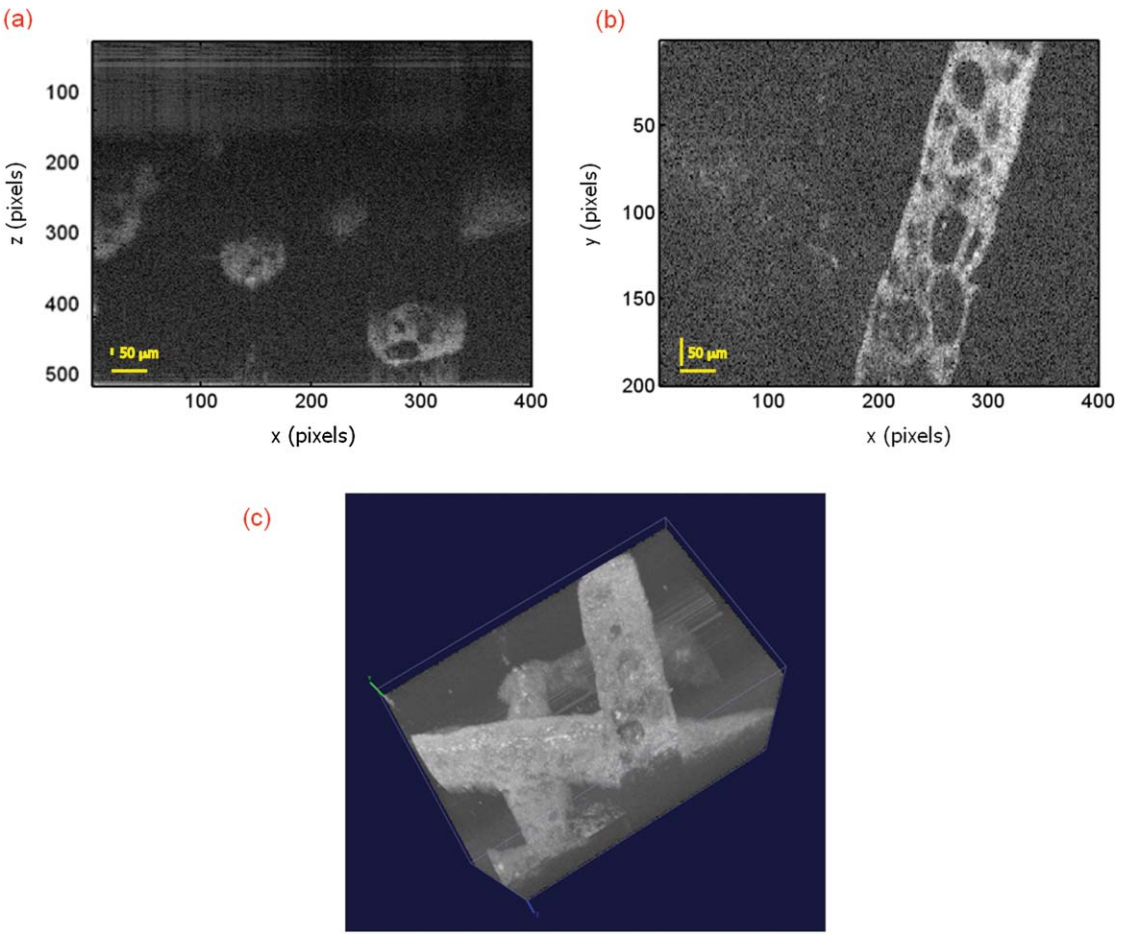

Fig. 5 (a) OCPM B scan of a blank scaffold. Porous fibers running in the direction perpendicular to the page were visible. (b) Reconstructed *en face* imaging from the acquisition of 200 B Scans in the *y* direction. (c) 3D projection of the scan data showing the 3D scaffold structure. Scanning steps [Ascan (*x*), Bscan (*y*)] in these pictures were set to 1.5 μm × 3 μm. Axial resolution in *z* is given by the OCPM axial resolution (i.e., 5 μm per pixel). Corresponding 50-μm scale bars were plotted.

4 Discussion

In this study, the existence of ADSC micromotion, which corresponded to vertical movements of a few nanometers in scale, was demonstrated with electric cell-substrate impedance sensing (ECIS). Cellular micromotion has been shown to be a marker of cell vitality[2,26] and did not occur for cells fixed in formalin. We calculated a power spectral density of ADSC impedance fluctuations that was typical of healthy cells.[27]

Using ECIS, the vertical displacement corresponding to Madin-Darby canine kidney cells (MDKC) cellular micromotion was estimated to be in the range of 1 to 20 nm,[26] when measured as an average over all the cells present on top of the electrodes. The sensitivity of the impedance measurements together with the large number of cells might account for a continuous recording of micromotion.

Once phase fluctuations on a cellular level with OCPM were measured, the resulting displacements were not averaged over an area of interest and corresponded to single cell displacements. Cell displacements on the order of 10 nm were found for adipose derived stem cells. We note that OCPM measurements were conducted at room temperature and cells could thus have experienced a reduction in cell micromotion as described in Ref. 2. Not all 2D live cell data revealed large phase fluctuations, and that can be attributed to the mode of data collection where the phase was measured over a very small area of the cell culture, i.e., along a line 3 μm thick and 600 μm long and over a limited time interval of 16.5 s. In comparison, the cellular micromotion measured with ECIS was averaged over a 250-μm electrode, increasing the chances to record cellular events. A direct comparison between ECIS micromotion and phase fluctuations was difficult at this stage and will require further statistical analysis.

OCPM has been previously used to record phase changes associated with cellular and intracellular events. In 2D, Joo et al.[28] have recently measured fast intracellular events in human epithelial ovarian cancer cells on a time scale of a few milliseconds. The system used in their study had a SNR of 37 db and was able to distinguish between Brownian and directional motions, both in emulsions and intracellularly.

Ellerbee et al.[29] and McDowell et al.[20] used a high spatial resolution OCPM to map the phase in 3D within, respectively, chick embryo cardiomyocytes and human breast cancer cells under mechanical stimuli. These studies used smaller acquisition times, on the order of a few milliseconds, and a smaller optical resolution. Consequently, they recorded different and

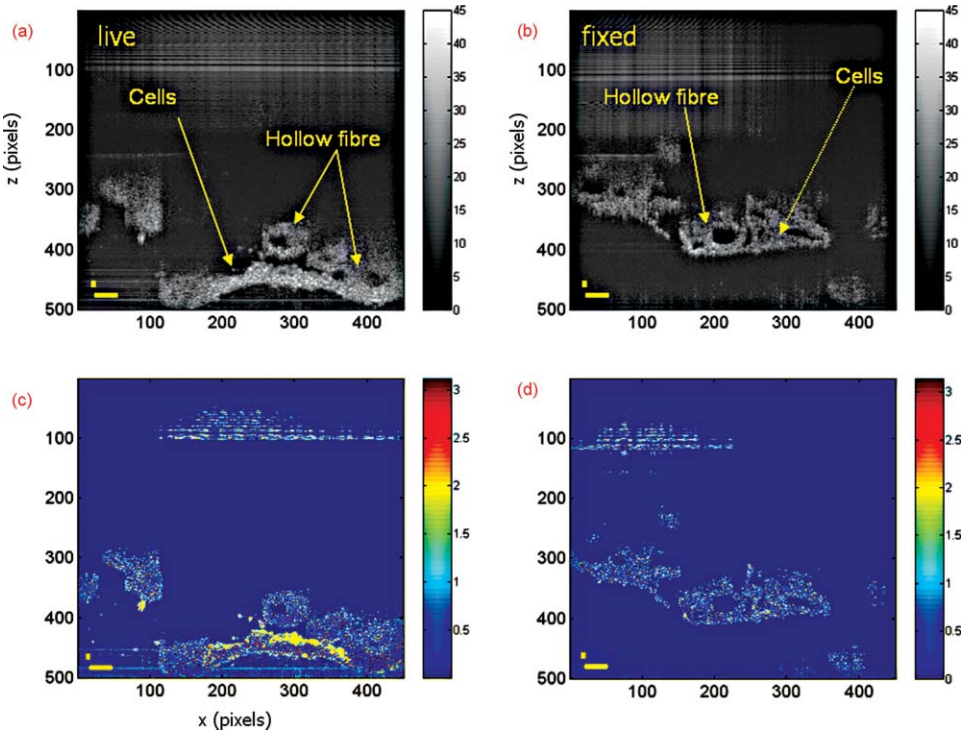

Fig. 6 (a) Intensity B scan for a live 3D cell culture. (b) Intensity B scan for a fixed 3D cell culture. The mean intensity over 50 B scans was plotted in all pictures. No clear contrast existed between the cells and scaffold material. Structurally round hollow fibers could be distinguished from the cells growing between them. Based upon mean intensity values, no differences could be made between live and fixed 3D samples. (c) Standard deviation map of the phase fluctuations for live 3D cell culture calculated over 50 B scans; and (d) $\delta\Phi$ standard deviation map for fixed 3D cell culture. Live cells were characterized by a higher standard deviation of $\delta\Phi$ when compared to fixed cells over the total acquisition time of 20.5 s. As a result, the cell-to-scaffold contrast was increased. Scanning steps in Ascan (x) in these pictures were set to 1.5 μm. Axial resolution in z is given by the OCPM axial resolution (i.e., 5 μm per pixel). Corresponding 50-μm scale bars were plotted.

greater sources of phase variations induced either by cardiac contractility or by an applied mechanical force. McDowell et al.[20] reported an SNR of 14 db and consequently focused on optical path differences greater than 20 nm.

Studies on a larger time scale were performed by Nezam et al.[30] They recorded, over several minutes (~20 min), the phase of fixed bovine pulmonary artery endothelial cells. They demonstrated an improvement in quantifying the absolute phase and the associated spatial variations of the optical path differences induced by cellular morphology, by applying a maximum likelihood estimator. They did not report imaging of phase fluctuations over this time scale, but mentioned that degradation of the SNR could be a source of noise for phase variation imaging. This SNR degradation could be a source of the fluctuations measured in fixed samples. Most of the studies to date focused on the mean value and standard deviation of the phase. In this study, we were interested in the maximum and the standard deviation of the first derivative of the phase, instead of measuring an absolute phase and optical path difference.

We have previously shown that our OCPM system produced high resolution imaging of ADSCs.[23] Herein, we have deliberately chosen to average the optical response of the cells over a larger beam spot to increase our chances to record phase fluctuations due to cellular micromotion. We also used a slower OCPM scanning rate to increase the SNR and to comply with the time scale of cellular micromotion.

Several quantitative phase imaging techniques have been developed and used to record phase fluctuations of cellular and intracellular events in 2D cultures. In this manuscript, we exploited the cross-sectional ability of optical coherence tomography to image 3D cell cultures. By using similar tools developed to assess cellular vitality in 2D, i.e., maximum and standard deviation of the phase fluctuations, we were able to discriminate in 3D between live and fixed cell cultures. Additionally, the cell-to-scaffold contrast was enhanced for live 3D culture when compared to standard intensity OCT imaging. In contrast to many standard viability assays, the method presented in this paper has the advantage of being real-time and label free.

Cellular motion was not necessarily the only source of phase fluctuations, and at this stage, we could not rule out local changes in optical properties arising from intracellular events that could have changed the local effective refractive index. However, the scale of the recorded events, similar to the scale of micromotion reported with ECIS, and the spatial spreading advocated for the cellular displacements being the cause of the phase fluctuations. In any case, phase fluctuations recorded with the OCPM were able to discriminate between live and fixed cells.

5 Conclusion

In this study, we presented an optical coherence phase microscope able to record optical phase fluctuations equivalent

to nanometer scale displacements. With electric cell-substrate impedance sensing, we have shown that live adipose derived stem cells were characterized by nanometer-scale cellular micromotion. Our results further indicated that OCPM was able to record phase fluctuations associated with live cells in both 2D and 3D. Considering the temporal and spatial scale of the fluctuations and their spatial spreading, it was likely that these fluctuations originated from cell motility. The findings presented in this study could be advantageously used to design real-time and label-free viability assays for 3D cell culture.

Acknowledgments

Pierre O. Bagnaninchi gratefully acknowledges support from the research councils UK for his fellowship and funding from EPSRC (EP/G030871/1). Christina Holmes was supported by NSERC Scholarship and by le «Fond Québécois de la Recherche sur la Nature et les Technologies»-Stages internationaux Award.

References

1. I. Giaever and C. Keese, "Micromotion of mammalian cells measured electrically," *Proc. Natl. Acad. Sci. U.S.A.* **88**(17), 7896–7900 (1991).
2. C. Lo, C. Keese, and I. Giaever, "Monitoring motion of confluent cells in tissue culture," *Exp. Cell Res.* **204**(1), 102–109 (1993).
3. F. Pampaloni, E. G. Reynaud, and E. H. K. Stelzer, "The third dimension bridges the gap between cell culture and live tissue," *Nat. Rev. Mol. Cell Biol.* **8**, 839–845 (2007).
4. W. L. Rice, D. L. Kaplan, and I. Georgakoudi, "Two-photon microscopy for non-invasive, quantitative monitoring of stem cell differentiation," *PLoS ONE* **5**(4), e10075 (2010).
5. S. Huang, A. A. Heikal, and W. W. Webb, "Two-photon fluorescence spectroscopy and microscopy of NAD(P)H and flavoprotein," *Biophys. J.* **82**(5), 2811–2825 (2002).
6. P. Marquet, B. Rappaz, P. J. Magistretti, E. Cuche, Y. Emery, T. Colomb, and C. Depeursinge, "Digital holographic microscopy: a noninvasive contrast imaging technique allowing quantitative visualization of living cells with subwavelength axial accuracy," *Opt. Lett.* **30**(5), 468–470 (2005).
7. B. Rappaz, P. Marquet, E. Cuche, Y. Emery, C. Depeursinge, and P. J. Magistretti, "Measurement of the integral refractive index and dynamic cell morphometry of living cells with digital holographic microscopy," *Opt. Express* **13**(23), 9361–9373 (2005).
8. N. Lue, W. Choi, G. Popescu, T. Ikeda, R. R. Dasari, K. Badizadegan, and M. S. Feld, "Quantitative phase imaging of live cells using fast Fourier phase microscopy," *Appl. Opt.* **46**(10), 1836–1842 (2007).
9. G. Popescu, L. P. Deflores, J. C. Vaughan, K. Badizadegan, H. Iwai, R. R. Dasari, and M. S. Feld, "Fourier phase microscopy for investigation of biological structures and dynamics," *Opt. Lett.* **29**(21), 2503–2505 (2004).
10. K. Jeong, J. J. Turek, and D. D. Nolte, "Speckle fluctuation spectroscopy of intracellular motion in living tissue using coherence-domain digital holography," *J. Biomed. Opt.* **15**(3), 030514 (2010).
11. S. A. Boppart, B. E. Bouma, C. Pitris, J. F. Southern, M. E. Brezinski, and J. G. Fujimoto, "In vivo cellular optical coherence tomography imaging," *Nature Med.* **4**(7), 861–865 (1998).
12. J. G. Fujimoto, "Optical coherence tomography for ultrahigh resolution in vivo imaging," *Nat. Biotechnol.* **21**(11), 1361–1367 (2003).
13. D. Huang, E. A. Swanson, C. P. Lin, J. S. Schuman, W. G. Stinson, W. Chang, M. R. Hee, T. Flotte, K. Gregory, C. A. Puliafito, and J. G. Fujimoto, "Optical coherence tomography," *Science* **254**(5035), 1178–1181 (1991).
14. S. A. Boppart, G. J. Tearney, B. E. Bouma, M. E. Brezinski, J. F. Southern, and J. G. Fujimoto, "Noninvasive assessment of the developing xenopus cardiovascular system using optical coherence tomography," *Proc. Natl. Acad. Sci. USA* **94**, 4256–4261 (1997).
15. W. Tan, A. Sendemir-Urkmez, L. J. Fahrner, R. Jamison, D. Leckband, and S. A. Boppart, "Structural and functional optical imaging of three-dimensional engineered tissue development," *Tissue Eng.* **10**(11–12), 1747–1756 (2004).
16. P. Bagnaninchi, Y. Yang, N. Zghoul, N. Maffulli, R. Wang, and A. Haj, "Chitosan microchannel scaffolds for tendon tissue engineering characterized using optical coherence tomography," *Tissue Eng.* **13**(2), 323–331 (2007).
17. P. O. Bagnaninchi, A. El Haj, and Y. Yang, "Continuous monitoring of tissue growth inside a perfusion bioreactor by optical coherence tomography," *Proc. SPIE* **6439**, 643903 (2007).
18. Y. Yang, A. Dubois, X. Qin, J. Li, A. El Haj, and R. Wang, "Investigation of optical coherence tomography as an imaging modality in tissue engineering," *Phys. Med. Biol.* **51**(7), 1649–1659 (2006).
19. M. A. Choma, A. K. Ellerbee, C. Yang, T. L. Creazzo, and J. A. Izatt, "Spectral-domain phase microscopy," *Opt. Lett.* **30**(10), 1162–1164 (2005).
20. E. J. McDowell, A. K. Ellerbee, M. A. Choma, B. E. Applegate, and J. A. Izatt, "Spectral domain phase microscopy for local measurements of cytoskeletal rheology in single cells," *J. Biomed. Opt.* **12**(4), 044008 (2007).
21. J. Zhang, B. Rao, L. Yu, and Z. Chen, "High-dynamic-range quantitative phase imaging with spectral domain phase microscopy," *Opt. Lett.* **34**(21), 3442–3444 (2009).
22. C. Joo, T. Akkin, B. Cense, B. H. Park, and J. E. de Boer, "Spectral-domain optical coherence phase microscopy for quantitative phase-contrast imaging," *Opt. Lett.* **30**(16), 2131–2133 (2005).
23. P. O. Bagnaninchi, "Combined optical coherence phase microscopy and impedance sensing measurements of differentiating adipose derived stem cells," *Proc. SPIE* **7566**, 756604 (2010).
24. R. Landers, A. Pfister, U. Hubner, H. John, R. Schmelzeisen, and R. Mulhaupt, "Fabrication of soft tissue engineering scaffolds by means of rapid prototyping techniques," *J. Mater. Sci.* **37**(15), 3107–3116 (2002).
25. A. M. Yousefi, C. Gauvin, L. Sun, R. W. DiRaddo, and J. Fernandes, "Design and fabrication of 3D-plotted polymeric scaffolds in functional tissue engineering," *Polym. Eng. Sci.* **47**(5), 608–618 (2007).
26. C. M. Lo, C. R. Keese, and I. Giaever, "Impedance analysis of MDCK cells measured by electric cell-substrate impedance sensing," *Biophys. J.* **69**(6), 2800–2807 (1995).
27. M. Tarantola, D. Schneider, E. Sunnick, H. Adam, S. Pierrat, C. Rosman, V. Breus, C. Sönnichsen, T. Basché, J. Wegener, and A. Janshoff, "Cytotoxicity of metal and semiconductor nanoparticles indicated by cellular micromotility," *ACS Nano* **3**(1), 213–222 (2009).
28. C. Joo, C. L. Evans, T. Stepinac, T. Hasan, and J. F. de Boer, "Diffusive and directional intracellular dynamics measured by field-based dynamic light scattering," *Opt. Express* **18**(3), 2858–2871 (2010).
29. A. K. Ellerbee, T. L. Creazzo, and J. A. Izatt, "Investigating nanoscale cellular dynamics with cross-sectional spectral domain phase microscopy," *Opt. Express* **15**(13), 8115–8124 (2007).
30. S. M. Motaghian Nezam, C. Joo, G. J. Tearney, and J. F. de Boer, "Application of maximum likelihood estimator in nano-scale optical path length measurement using spectral-domain optical coherence phase microscopy," *Opt. Express* **16**(22), 17186–17195 (2008).